The 2010 IEEE/RSJ International Conference on
Intelligent Robots and Systems
October 18-22, 2010, Taipei, Taiwan

Force Control of a Robot for Wrist Rehabilitation: towards Coping with Human Intrinsic Constraints

Nevio Luigi Tagliamonte, Domenico Formica, Maria Scorcia, Domenico Campolo, Eugenio Guglielmelli

Abstract— **This work proposes a mechatronic solution to increase the back-drivability of a state-of-the art robot for wrist neurorehabilitation. The final goal is to reduce robot mechanical impedance in order to cope with intrinsic kinematic constraints, which are adopted by the human brain to solve redundancy during pointing tasks with the wrist. The handle of the robot has been provided with a load cell and a direct force control scheme has been implemented to minimize the interaction forces/torques between the user and the robot. To this aim gravity, inertia and friction of the more proximal DOF of the robot (relative to Pronation/Supination (PS) movements) have been estimated and compensated for. The proposed solution resulted in a 70% reduction of the end-point perceived inertia in PS DOF as well as in a decrease of torques exerted by the user during both 1-DOF and 3-DOFs tasks. The average reduction of interaction torques is around 81% and 78% respectively. This work constitutes an important starting point for the analysis of the effect that different levels of robot transparency could have on the human neural constraints adopted during redundant tasks, such as pointing movements with the wrist.**

I. INTRODUCTION

Rehabilitation robotics has become an emerging field in recent years and the potentialities of robot-mediated motor therapy is being widely investigated [1]–[4].

During traditional neurorehabilitation sessions the role of the patient is quite passive and the participation of the high-level structures of his nervous system are limited. On the other hand, robotic therapy allows subjects to perform voluntary movements, thus promoting neurogenesis and neuroplasticity, and optimizing the functional recovery after neurological injuries [5], [6].

Rehabilitation robots have to provide assistance as needed, so that to not perturb voluntary movements of the users, and to help completing the tasks that they are not able to perform autonomously. In this sense a high back-drivability, i.e. a low perceived impedance during retrograde motion, is of crucial importance. The technological choices in the design of mechanical structure and control strategies of robots strictly interacting with humans, have to face several issues, such as safety, dynamical adaptability and biomechanical compatibility [7]. Moreover, it has been shown that rehabilitation machines have to comply not only with 'hard' (*biomechanical*) constraints but also with 'soft' (*instrinsic*) constraints of neural origin, which are adopted by the brain to solve kinematic redundancy and to implement strategies for motor efficiency [8].

The first historical examples (1847) of such intrinsic constraints were found in the oculomotor system by Donders. He found that, for a given steady gaze direction, physiological eye configurations are described by a 2-dimensional surface embedded into the 3-dimensional space of eye configurations (Donders' law) [9]. Nowadays, it has been demonstrated that such a law is actively implemented by a neural mechanism, and it is also well applied to limb movements [8], [10].

Recent studies demonstrated that Donders' law applies also to wrist movements during pointing tasks (in which the three DOFs of the wrist are redundant) [11]. This study was conducted measuring wrist orientations during pointing movements using a lightweight 'hand-held device', which introduces negligible perturbation to the physiological movements. The three dimensional rotations vectors resulted well fitted by quadratic (Donders') surfaces, whose curvature expresses inter-subjects differences in motor strategies, thus denoting a 'personal style' in solving redundancy [11].

The same analysis was conducted in [12] with subjects performing similar pointing tasks while interacting with the InMotion^3 system (Interactive Motion Technologies, Inc.), a the state-of-the-art robot for wrist neurorehabilitation, specifically designed to comply with the biomechanical constraints, and providing a high degree of back-drivability [13]. In this case no statistically significant difference was found between subjects, suggesting that the robot flattens out any personal intrinsic motor strategy (in particular the most proximal joint, for pronation/supination movements, is perceived as too heavy by the subjects during the task). In other terms, the robot perturbs voluntary movements of the subjects, despite its low mechanical impedance (it has been shown to not be transparent enough to comply with the intrinsic constraints of neural origin).

The goal of this work is to provide the handle of the InMotion^3 wrist robot with a load cell and to implement a direct force control scheme to improve the back-drivability of the system. This kind of mechatronic approach has been already validated in [14] on the MIT-MANUS robot [1] (InMotion^2 system by Interactive Motion Technologies, Inc.) in both simulation and experimental tests. In [14] a reduction of (mean and maximum) forces exerted by a subject during planar pointing tasks has been verified in different operative conditions, demontrating the effectiveness of the chosen force control algorithm in improving the system transparency. In this work the handle of the InMotion^3 wrist robot has been sensorized; inertia, friction and gravitational

N. L. Tagliamonte, D. Formica, M. Scorcia and E. Guglielmelli are with the Laboratory of Biomedical Robotics and Biomicrosystems, Faculty of Biomedical Engineering, Università Campus Bio-Medico di Roma, Via Álvaro del Portillo, 21 - 00128 Roma, Italy.

D. Campolo is with the School of Mechanical & Aerospace Engineering, Nanyang Technological University, 50 Nanyang Avenue, Singapore.

Corresponding author: n.tagliamonte@unicampus.it

effects of the pronation/supination DOF have been estimated to be actively compensated with a pure force control algorithm. The performance of the robot have been analyzed with and without the force control to verify the reduction of the perceived mechanical impedance. Moreover, the reduction of forces/torques required to a subject to perform two different kinds of tasks (involving respectively 1 or 3 DOFs movements) has also been measured.

The validation of this control scheme is the first step for a future work on testing the effect that different levels of transparency of the robot have on the human motor strategies. The relation between robot back-drivability and human motor control could possibly be useful in defining indications for the design of a new generation of rehabilitative robots, able to comply with constraints of neural origin.

II. InMotion^3 wrist robot

The InMotion^3 system [13] has three active DOFs: Pronation/Supination (PS), Abduction/Adduction (AA) and Flexion/Extension (FE). A differential mechanism is used to achieve AA and FE movements; PS rotations entail the sliding along a curve guide of the housing comprising the differential gearing and the AA and FE actuators (Fig. 1).

In [13] a quantification of the three axis inertia, friction and gravity terms is provided showing that PS values are one order of magnitude higher with respect to the two other DOFs.

At the basis of the handle a linear slider and a revolute joint allow two other passive DOFs for a further adaptation of the robot to the axes of rotation of the human wrist (Fig. 1).

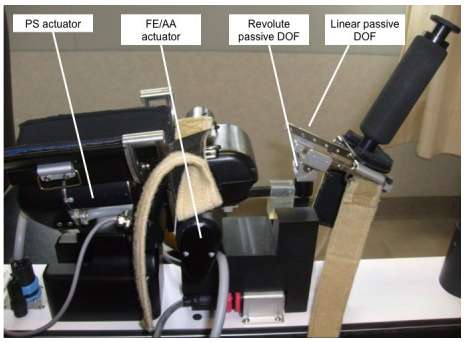

Fig. 1. InMotion^3 wrist robot [13].

In this work we sensorized the robot handle, in order to implement a direct force control for the reduction of end-point impedance of the PS degree of freedom. To this aim we decided to remove the linear slider and the passive revolute joint, whose movements could not be measured/controlled, and to collocate a load cell to the basis of the hand effector (Fig. 2). A 6 DOFs JR3 force/torque sensor (20E12A4-I25-EF 100N5, JR3 Inc.) with external electronics was used. The six analog outputs of the sensor were directly connected to an acquisition board already present on the robot, which automatically synchronizes external signals with the 200 Hz control software. The sampled signals have been multiplied by a calibration and decoupling matrix, provided by the manufacturer of the sensor.

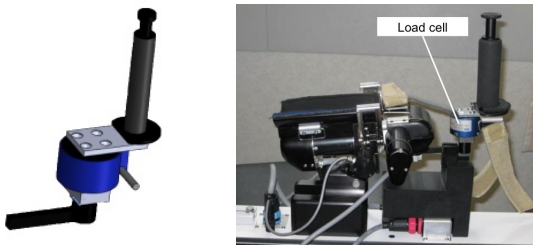

Fig. 2. Integration of the force/torque sensor in the InMotion^3 system. The linear slider and the passive revolute joint have been removed.

III. Force control

The control algorithm proposed in this work is adapted from [15], [16]. It compensates robot dynamics (gravity, inertia and friction) and minimizes the end-point interaction force since a zero reference is imposed. This strategy allows the robot to 'follow' subjects' movements, making them appear almost free.

The equation of robot dynamics[1] can be expressed as:

$$\boldsymbol{B}(\boldsymbol{q})\ddot{\boldsymbol{q}} + \boldsymbol{b}\dot{\boldsymbol{q}} + \boldsymbol{g}(\boldsymbol{q}) + \boldsymbol{J}^T(\boldsymbol{q})\boldsymbol{F}_{int} = \boldsymbol{\tau} \tag{1}$$

where $\boldsymbol{F}_{int}$ represents the 6×1 vector of the generalized forces exerted by the user (respect to the base frame), $\boldsymbol{b}$ is a 3×3 diagonal matrix of constant friction coefficients, $\boldsymbol{B}(\boldsymbol{q})$ is the 3×3 inertia matrix, $\boldsymbol{J}^T(\boldsymbol{q})$ is the 3×6 transposed Jacobian matrix, $\boldsymbol{g}(\boldsymbol{q})$ is the 3×1 gravity term and $\boldsymbol{\tau}$ is the 3×1 vector of control torques. Relation (1) is composed by three scalar equations, which refer to PS, AA and FE DOFs respectively; thus the vector of joint coordinates is $\boldsymbol{q} = [q_{PS}\ q_{AA}\ q_{FE}]^T$.

The implemented control law is:

$$\boldsymbol{\tau} = \hat{\boldsymbol{b}}\dot{\boldsymbol{q}} + \hat{\boldsymbol{g}}(\boldsymbol{q}) + \boldsymbol{J}^T(\boldsymbol{q})\boldsymbol{F}_{sens} + \hat{\boldsymbol{B}}(\boldsymbol{q})\boldsymbol{K}_P\boldsymbol{J}^T(\boldsymbol{q})(\boldsymbol{F}_d - \boldsymbol{F}_{sens}) \tag{2}$$

where the symbol $\hat{}$ indicates an estimation of the corresponding vector or matrix, $\boldsymbol{F}_{sens}$ indicates the 6×1 vector of generalized forces measured by the load cell and $\boldsymbol{K_P}$ is a 3×3 positive-definite diagonal gain matrix. A block scheme of control law in (2) is presented in Fig. 3.

Force error can be indicated as $\boldsymbol{e}_f = \boldsymbol{F}_d - \boldsymbol{F}_{sens}$, where $\boldsymbol{F}_d$ is the desired interaction force (which in our application is set to zero). By substituting (2) in (1), and assuming that robot dynamical parameters have been perfectly estimated, the force error dynamics becomes:

$$\boldsymbol{e}_f = \boldsymbol{M}\ddot{\boldsymbol{q}} \tag{3}$$

If $\boldsymbol{F}_d$ is set to zero, equation (3) indicates that the system behaves like a free body with mass $\boldsymbol{M} = \boldsymbol{K}_P^{-1}$, so that

[1]Coriolis and centrifugal effects have been neglected because of the low values of velocity involved in the wrist pointing tasks. Hereafter vectors and matrices will be reported in **bold** font.

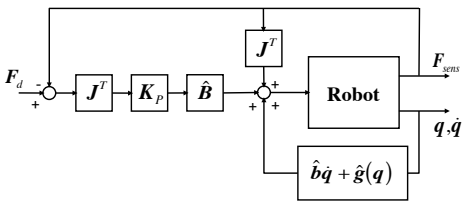

Fig. 3. Block diagram of force control scheme in (2); the 'Robot' block represents the first term of equation (1).

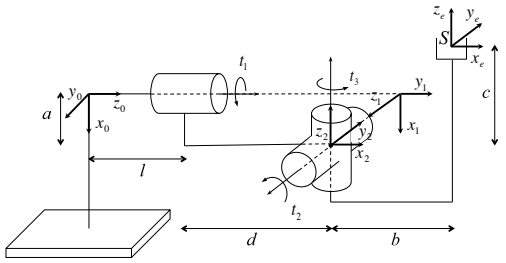

Fig. 4. Schematic representation of the robot kinematics (without the passive DOFs); frames of reference are selected using the Denavit-Hartenberg convention. We measured $a = 0.062$ m, $b = 0.158$ m, $c = 0.022$ m, $d = 0.120$ m, $l = 0.100$ m.

increasing proportional gain (within stability margins) will reduce the end-point perceived inertia. Force control in (2) has been implemented only for the PS DOF since the AA and FE DOFs are already highly back-drivable (their mechanical impedance is one order of magnitude smaller than the one of PS DOF [13]); for this reason the control torques can be written as follows:

$$\begin{cases} \tau_{PS} = \boldsymbol{\tau}[1\ 0\ 0]^T \\ \tau_{AA} = 0 \\ \tau_{FE} = 0 \end{cases} \tag{4}$$

with

$$\tau_{PS} = b_{PS}\dot{q}_{PS} + \tau^g_{PS} + \\ + [\boldsymbol{J}^T(\boldsymbol{q})\boldsymbol{F}_{sens} + \hat{\boldsymbol{B}}(\boldsymbol{q})\boldsymbol{K}_P\boldsymbol{J}^T(\boldsymbol{q})(\boldsymbol{F}_d - \boldsymbol{F}_{sens})][1\ 0\ 0]^T \tag{5}$$

where $\tau^g_{PS} = g_{PS}\sin(q_{PS})$ and b_{PS} are the gravity term and the friction coefficient of the PS DOF, respectively. The implementation of the control scheme in (5) required the calculation of the robot kinematic operators and the estimation of its dynamical properties.

A. Robot kinematic operators

Since the robot native control is implemented only in the joints space, the calculation of the Jacobian matrix $\boldsymbol{J}(\boldsymbol{q})$, and of its transpose $\boldsymbol{J}^T(\boldsymbol{q})$, was necessary to map the forces/torques measured in the operative space in the corresponding actions on the joints. A schematic representation of the robot kinematics (without considering the passive DOFs) is provided in Fig. 4. Denavit-Hartenberg convention was used to select the frames of reference.

In addition the adjoint transformation [17] was used to map the vector of generalized forces from the sensor coordinate frame to the global reference system (base frame): $\boldsymbol{F}_{sens} = \boldsymbol{Ad}_g\boldsymbol{F}^S_{sens}$ (the superscript S refers to the sensor reference frame, see Fig. 4).

B. Gravity term estimation

To estimate the gravity term for the PS DOF, a correlation between different static configurations and the torques required to hold the robot in those positions was performed.

It is important to note that tests were carried out with AA and FE DOFs locked (being the actuators commanded to maintain their 0 reference position through high gains PD position control), thus neglecting the contribution of changes in AA and FE configurations on the PS gravity term.

The robot was commanded to reach 10 positions (from -0.6 rad to +0.6 rad with respect to its rest position); PS actuator torques exerted to maintain these rotations in static conditions were evaluated. Figure 5 shows an example of the PS torque and angle patterns during one estimation test of gravity term.

A linear regression between PS torque and the sin of the PS rotation was calculated. In Fig. 6 the collected data (static PS angles and torques for the 5 trials) are shown together with the best fitting curve.

The slope of the linear curve in Fig. 6, averaged on the 5 trials, was found to be $g_{PS} = 2.254 \pm 0.009$ Nm, with a mean R^2 of 0.980.

C. Inertia and friction estimation

To estimate inertia and friction terms the robot was back-driven by one of the authors to perform few rapid oscillating movements. The PS motor compensated the gravity effect (on the basis of the estimation reported in III-B) and the AA and FE actuators were commanded to maintain their rest positions through high gains PD control; in these conditions forces/torques exerted on the hand effector were recorded and their effect on the PS DOF was calculated as follows:

$$\tau^{PS}_{sens} = [\boldsymbol{J}(\boldsymbol{q})^T\boldsymbol{Ad}_g\boldsymbol{F}^s_{sens}][1\ 0\ 0]^T. \tag{6}$$

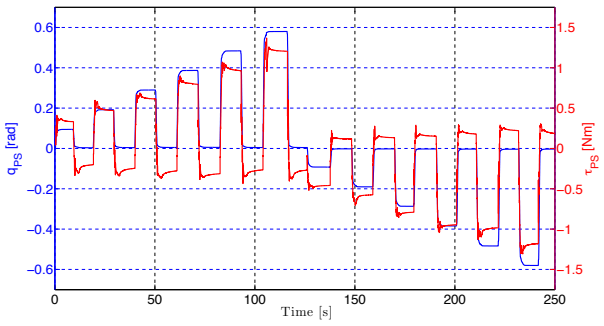

Fig. 5. PS torque and angle patterns during one test for the gravity term estimation. Commanded angles varied from -0.6 rad to +0.6 rad with respect to the robot rest configuration.

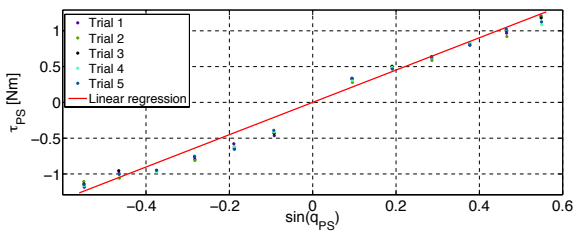

Fig. 6. Linear regression between τ_{PS} and $\sin(q_{PS})$ static values for the estimation of the PS gravity term. The fitting curve slope is mediated on 5 trials. The resultant gravitational term is $\tau^g_{PS} = g_{PS}\sin(q_{PS}) = 2.254\sin(q_{PS})$.

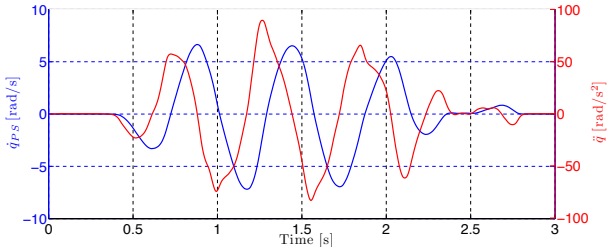

Fig. 7. Velocity and acceleration profiles for one representative trial of the inertia and friction identification procedure. These values are obtained by manually back-driving the handle of the robot while locking AA and FE DOFs and compensating the gravity effect for the PS DOF.

In Fig. 7 velocity and acceleration profiles for one representative trial are shown.

We estimated the inertia and friction terms for the PS DOF by regressing the τ^{PS}_{sens} reported in (6) with angular velocities and accelerations of the PS DOF, as reported in the following:

$$\tau^{PS}_{sens} = \tau^0_{PS} + b_{PS}\dot{q}_{PS} + B_{PS}\ddot{q}_{PS} \tag{7}$$

The multivariable linear regression reported in (7) was calculated on 5 trials; the best fitting plane is shown in Fig. 8. We found $\tau^0_{PS} = 0.219 \pm 0.049$ Nm, $b_{PS} = 0.055 \pm 0.005$ Nm·s/rad and $B_{PS} = 0.012 \pm 0.001$ kg·m^2 with a mean R^2 of 0.942.

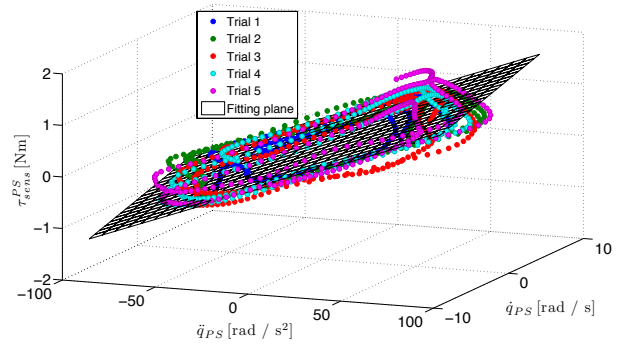

Fig. 8. Multivariable linear regression for PS inertia and friction estimation as reported in (7). Considering the values averaged on 5 trials, we found $\tau^0_{PS} = 0.219 \pm 0.049$ Nm, a viscous friction $b_{PS} = 0.055 \pm 0.005$ Nm·s/rad and an inertia $B_{PS} = 0.012 \pm 0.001$ kg·m^2, with a mean R^2 of 0.942.

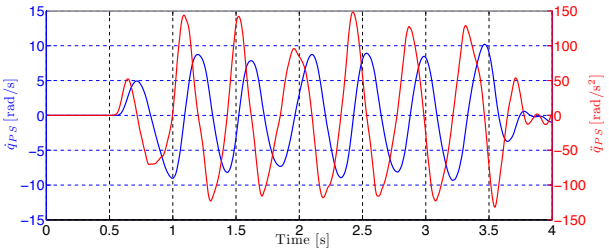

Fig. 9. Velocity and acceleration profiles for one representative trial of the mechanical impedance evaluation test with force control active on PS DOF. These values are obtained by manually back-driving the handle of the robot while locking AA and FE DOFs.

IV. Validation Results

In this section the effectiveness of the force control in (5) in improving the transparency of the robot is tested. First, the reduction of the end-point mechanical impedance in the PS DOF, due to the action of the force control has been estimated; then the reduction of forces/torques exerted by three subjects while performing two kinds of pointing tasks were analyzed, comparing the cases of uncontrolled robot, gravity-compensated robot, and force-controlled robot.

A. Reduction of end-point inertia

To evaluate the perceived mechanical impedance with the action of the force control, the same procedure described in section III-C was followed. In particular the proportional gain of the force control was set to 250 kg^{-1}m^{-2}.

In Fig. 9 velocity and acceleration profiles for one trial are shown.

The multivariable linear regression reported in (7) was calculated on 5 trials; the best fitting plane is shown in Fig. 10. We found $\tau^0_{PS} = -0.059 \pm 0.043$ Nm, $b_{PS} = -0.002 \pm 0.002$ Nm·s/rad and $B_{PS} = 0.0037 \pm 0.0001$ kg·m^2 with a mean R^2 of 0.980. The negative value of friction suggest that an overestimation of this parameter was made.

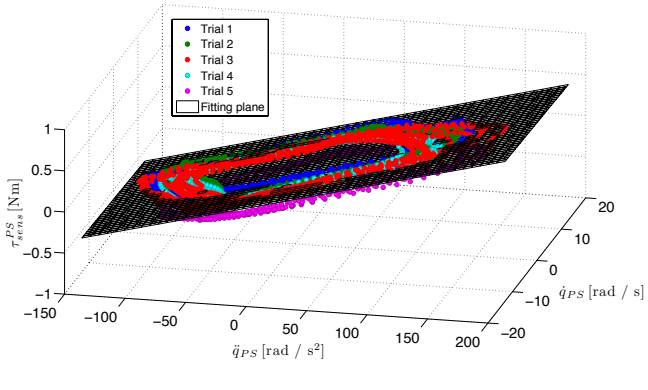

Fig. 10. Multivariable linear regression for PS mechanical impedance estimation with force-controlled robot. Considering the values averaged on 5 trials, we found $\tau^0_{PS} = -0.059 \pm 0.043$ Nm, a viscous friction $b_{PS} = -0.002 \pm 0.002$ Nm·s/rad and an inertia $B_{PS} = 0.0037 \pm 0.0001$ kg·m^2, with a mean R^2 of 0.980. A reduction of about 70% of perceived inertia was obtained.

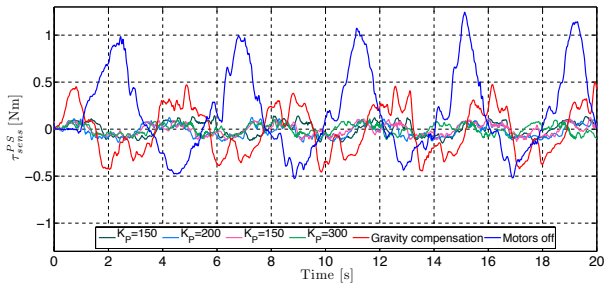

Fig. 11. τ^{PS}_{sens} pattern for 1-DOF (PS) tasks, performed by one representative subject, in three different conditions: uncontrolled robot (motors off), gravity-compensated robot and force-controlled robot with different values of K_P.

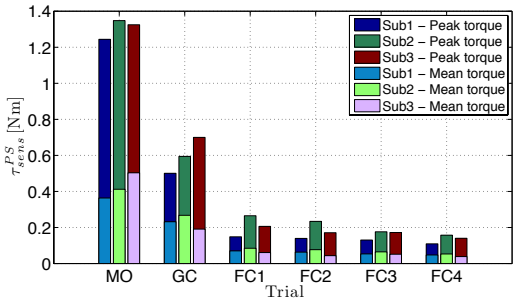

Fig. 12. τ^{PS}_{sens} peak and mean values for 1-DOF (PS) tasks on three subjects (Sub1-3). Five conditions are reported: Motors Off (MO); Gravity Compensation (GC); Force Control $K_P = 150$ kg^{-1}m^{-2} (FC1); Force Control $K_P = 200$ kg^{-1}m^{-2} (FC2); Force Control $K_P = 250$ kg^{-1}m^{-2} (FC3); Force Control $K_P = 300$ kg^{-1}m^{-2} (FC4).

Anyway, this value can be considered negligible since it was found to be not statistically different from 0.

Of note, the implemented force control causes a reduction of the inertia of about 70% with respect to the case with simple gravity compensation (section III-B).

B. Reduction of forces/torques exerted by the user

In this section PS torques (τ^{PS}_{sens}, as in (6)) exerted by three healthy subjects (Sub1-3) to perform a 1-DOF (Pronation/Supination) task and a 3-DOFs task are reported for three different conditions: uncontrolled robot (Motors Off, MO), Gravity-Compensated robot (GC) and Force-Controlled robot (FC).

1) Pronation/Supination (PS) task: During this 1-DOF task, three healthy subjects were asked to alternately reach 2 points displayed on a monitor on the left and right sides of a starting central point, only using the PS DOF (AA and FE DOFs were constrained in their rest positions through high gains PD position control).

Fig. 11 shows the PS torque (6) exerted by one representative subject in the different testing conditions. The only gravity compensation reduces the torques required to perform the task with respect to the case of motors off; further decrease of the torque in the case of the force-controlled robot can be noticed. Fig. 12 reports the peak and mean values of the PS torque for the 1-DOF trials on the three subjects.

It can be seen that these values slightly decrease increasing the gain K_P although no major changes occur. In case of $K_P = 300$ kg^{-1}m^{-2} the peak torque decreases of the 90% while the mean torque of the 81% with respect to the uncontrolled robot case. Gravity compensation only causes a reduction of the 54% and 46% of the peak and mean torques respectively. Of note, the force control ($K_P = 300$ kg^{-1}m^{-2}) reduces the peak and mean torques of 77% and 65% respectively, with respect to the gravity compensated condition.

2) 3-DOFs task: During this 3-DOFs task, three healthy subjects were asked to perform pointing movements with the wrist from the center of the workspace to 8 peripheral points arranged in a circle displayed on the monitor; this is also a typical rehabilitation exercise often indicated as *clock* game,

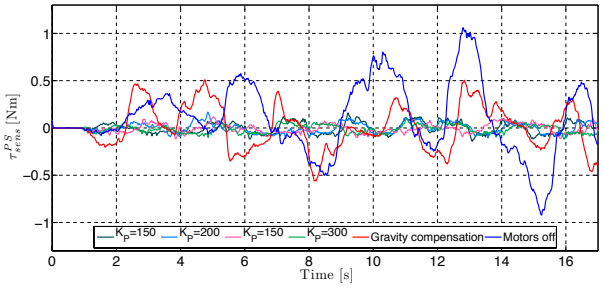

Fig. 13. τ^{PS}_{sens} pattern for 3-DOFs tasks, performed by one representative subject, in three different conditions: uncontrolled robot (motors off), gravity-compensated robot and force-controlled robot with different values of K_P.

which has been used in [12] to test the effect of the robot on human motor strategies.

Fig. 13 shows the PS torque (6) exerted by one representative subject in the different testing conditions. Also in this case gravity compensation lowers the PS torques with respect to the case of uncontrolled robot and force control improves this effect.

Fig. 14 reports the peak and mean values of the PS torque for the trials on the three subjects. No major changes occur with the gain increasing. In case of $K_P = 300$ kg^{-1}m^{-2} the peak torque decreases of the 80% and the mean torque decreases of the 78% with respect to the uncontrolled robot case. With gravity compensation the peak and mean torques only decrease of the 5.6% and 5.4% respectively; thus the force control ($K_P = 300$ kg^{-1}m^{-2}) reduces the peak and mean torques of 79% and 77% respectively, with respect to the gravity compensated condition.

An overall view of the results obtained is presented in Table I.

V. CONCLUSIONS AND FUTURE WORKS

A. Conclusions

In this work a solution to improve back-drivability of a state-of-the-art robot for wrist neurorehabilitation is presented. The handle of the robot was provided with a load cell and a 0 reference direct force control scheme was

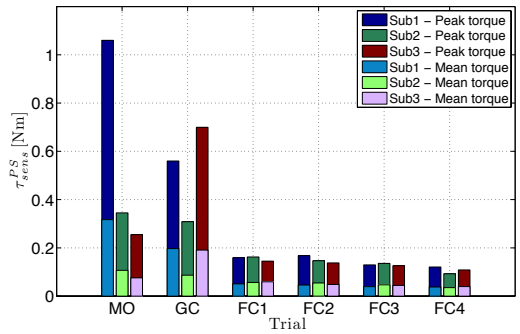

Fig. 14. τ_{sens}^{PS} peak and mean values for 3-DOFs tasks on three subjects (Sub1-3). Five conditions are reported: Motors Off (MO); Gravity Compensation (GC); Force Control $K_P = 150$ kg^{-1}m^{-2} (FC1); Force Control $K_P = 200$ kg^{-1}m^{-2} (FC2); Force Control $K_P = 250$ kg^{-1}m^{-2} (FC3); Force Control $K_P = 300$ kg^{-1}m^{-2} (FC4).

TABLE I

τ_{sens}^{PS} PEAK AND MEAN VALUES FOR 1-DOF (PS) AND 3-DOFS TASKS

	Peak torque [Nm]		*Mean torque* [Nm]	
	PS	3-DOFs	PS	3-DOFs
MO	1.306 ± 0.055	0.553 ± 0.441	0.427 ± 0.071	0.167 ± 0.131
GC	0.598 ± 0.099	0.522 ± 0.198	0.230 ± 0.038	0.158 ± 0.062
FC1	0.206 ± 0.059	0.155 ± 0.009	0.072 ± 0.012	0.056 ± 0.004
FC2	0.181 ± 0.048	0.151 ± 0.185	0.061 ± 0.017	0.049 ± 0.004
FC3	0.162 ± 0.028	0.139 ± 0.021	0.057 ± 0.007	0.043 ± 0.004
FC4	0.135 ± 0.024	0.108 ± 0.014	0.081 ± 0.066	0.037 ± 0.002

implemented to minimize the perturbations in the user natural movements of the pronation/supination DOF.

Dynamical parameters of the PS DOF were estimated and compensated for in the control law. Inertia and friction were identified correlating the torque exerted to back-drive the robot and the velocity/acceleration produced; the gravity term was estimated on the basis of the torques exerted by the robot to maintain a set of static configurations.

We showed that the implemented force control law caused a net increasing of the robot transparency. The PS inertial effect was reduced of about 70% and friction became negligible (considering a fixed exemplification value of the control gain). Gravity compensation lowered the mean PS torque required to a healthy subject to perform 1- and 3-DOFs tasks of less than 40%. The effect of the force control was to minimize the mean torque exerted by the subject till the 90% and 80% (respectively for 1- and 3-DOFs tasks) of the value needed in the case of uncontrolled robot.

Results show that an increased level of back-drivability was obtained with the proposed solution.

B. Future Works

In [12] it was demonstrated that the InMotion^3 system was note able to cope with intrinsic ('soft') constraints of neural origin, used by the brain to solve redundancy during pointing tasks with the wrist. Starting from the results of this work it will be possible to verify if the force-controlled robot is capable to respect the human physiological motor strategies and which can be the effects of different levels of transparency. Our future works will be focused on demonstrating that Doders' surfaces, fitting wrist rotations during pointing tasks with the robot, will approximate, and ideally match, the ones obtained in free space.

VI. ACKNOWLEDGMENTS

This work was partly funded by the FP7 FET Proactive Initiative 'Embodied Intelligence', project no. ICT-2007.8.5-231451 - EVRYON and by the FP7-ICT project, no. ICT-2007.3.2-231722 - IM-CLeVeR.

REFERENCES

[1] H. I. Krebs, N. Hogan, M. L. Aisen, B.T. Volpe, "Robot-aided neurorehabilitation", *IEEE Transactions on Rehabilitation Engineering*, 6, pp. 75–87, 1998.

[2] C. G. Burgar, P. S. Lum, P. C. Shor, and H. F. M. Van der Loos, "Development of robots for rehabilitation therapy: The Palo development of robots for rehabilitation therapy: The Palo Alto Stanford experience, Journal of rehabilitation research and development, vol. 37(6), pp. 663–673, 2000.

[3] P. S. Lum, D. J. Reinkensmeyer, R. Mahoney, W. Z. Rymer, and C. G. Burgar, "Robotic devices for movement therapy after stroke: Current status and challenges to clinical acceptance, *Topics in stroke rehabilitation*, vol. 8(4), pp. 40–53, 2002.

[4] G. Colombo, R. Riener, and L. Lünenburger, "Human-centered robotics applied to gait training and assessment, *Journal of rehabilitation research and development*, vol. 43(5), pp. 679–694, 2006.

[5] J. D. Schaechter, "Motor rehabilitation and brain plasticity after hemiparetic stroke", *Prog. Neurobiol.*, 73(1), pp. 61–72, 2004.

[6] R. Teasell, N. A. Bayona, J. Bitensky, "Plasticity and reorganization of the brain post stroke", *Topics in Stroke Rehabilitation*, 12(3), pp. 11–26, 2005.

[7] D. Reinkensmeyer, N. Hogan, H. I. Krebs, S. L. Lehman, P. S. Lum, "Rehabilitators, robots and guides: new tools for neurological rehabilitation", In: *Biomechanics and Neural Control of Posture and Movement*, Eds. J. Winters, P. E. Crago, Springer-Verlag, pp. 516–534, 2000.

[8] D. G. Liebermann, A. Biess, J. Friedman C. C. A. M. Gielen, T. Flash, "Intrinsic joint kinematic planning. I: Reassessing the Listing's law constraint in the control of three-dimensional arm movements", *Exp. Brain. Res.*, 171, pp. 139–154, 2006.

[9] D. Tweed and T. Vilis, "Geometric Relations of Eye Position and Velocity Vectors during Saccades",*vision Res.*, 30(1), pp. 111–127, 1990.

[10] M. Fetter, T. Haslwanter, H. Misslich, D. Tweed, "Threedimensional Kinematics of the Eye, Head and Limb Movements", Amsterdam, The Netherlands, Harwood Academic Publisher, 1997.

[11] D. Campolo, D. Formica, E. Guglielmelli, F. Keller, "Kinematic analysis of the human wrist during pointing tasks", *Experimental Brain Research*, 2009.

[12] D. Campolo, D. Accoto, D. Formica, E. Guglielmelli, "Intrinsic constraints of neural origin: Assessment and application to rehabilitation robotics", *IEEE Transaction on Robotics*, 25, pp. 492–501, 2009.

[13] H. I. Krebs, B. T. Volpe, D. Williams, J. Celestino, S. K. Charles, D. Lynch and N. Hogan, "Robot-aided neurorehabilitation: a robot for wrist rehabilitation", *IEEE Transactions on Rehabilitation Engineering*, 15, pp. 327–335, 2007.

[14] N. L. Tagliamonte, D. Formica, D. Campolo, E. Guglielmelli, "Coping with Intrinsic Constraints of Neural Origin in the Design of Rehabilitation Robots: a Preliminary Study, *IEEE/EMBS Conference on Neural Engineering*, Antalya, Turkey, 2009, pp. 124-127.

[15] O. Khatib, "Inertial properties in robotics manipulation: an object-level framework", *International Journal of Robotics Research*, 14, pp. 19–36, 1995.

[16] R. Volpe, P. Khosla, "A theoretical and experimental investigation of explicit force control strategies for manipulators", *IEEE Trans. Autom. Control*, 38(11), pp. 1634–1650, 1993.

[17] R. M. Murray, Z. Li, and S. S. Sastry, "A Mathematical Introduction to Robotic Manipulation", Boca Raton, FL: CRC Press, 1994.